ADVANCED MATERIALS INTERFACES
www.advmatinterfaces.de

FULL PAPER

Single Nozzle Electrospinning Synthesized MoO_2@C Core Shell Nanofibers with High Capacity and Long-Term Stability for Lithium-Ion Storage

Zhi Chen, Ting Yang, Huimin Shi, Taihong Wang, Ming Zhang, and Guozhong Cao*

MoO_2@C core shell nanofibers are synthesized via a simple electrospinning method with a single nozzle. The formation mechanism of MoO_2@C core shell nanofibers is investigated in detail and it is discovered that the phase-segregation phenomenon may be the main driving force of thermodynamics to form MoO_2@C core shell nanofibers, and the high temperature as the dynamic factor can accelerate the formation of these core shell nanofibers. The carbon shell of the MoO_2@C core shell nanofibers acts as both conductive bond to increase electrical conductivity and structural skeleton to maintain the integrity of MoO_2 during Li^+ insertion/extraction to achieve both high specific capacity and good cyclic stability. So as an anode for lithium-ion batteries, the MoO_2@C core shell nanofiber electrode exhibits high specific capacity and extraordinary lifetime even at a large current density. Their reversible capacities are 665 mA h g^{-1} in the 600th cycle at 0.5 A g^{-1}. Even at a high current density of 1 A g^{-1}, a capacity of 537 mA h g^{-1} is obtained after 600 cycles. The present work may provide a facile and broadly applicable way for the fabrication and utilization of metal oxide/carbon core shell composites in fields of batteries, catalysts, and fuel cells.

1. Introduction

Although lithium-ion batteries (LIBs) have been becoming a break-through for energy storage, commercial graphite as an anode for LIBs has not satisfied the high efficiency energy demand in electric vehicles or hybrid electric vehicles in future.[1–5] Therefore developing novel and appropriate electrode materials with high energy density, long cycle life, and low cost is essential to improve the performance of batteries for electric vehicles.[5–13]

Dr. Z. Chen, Dr. T. Yang, Dr. H.-M. Shi,
Prof. T.-H. Wang, Prof. M. Zhang
Key Laboratory for Micro-Nano Optoelectronic Devices of Ministry of Education
School of Physics and Electronics
State Key Laboratory for Chemo/Biosensing and Chemometrics
Hunan University
Changsha 410082, China
E-mail: zhangming@hnu.edu.cn
Prof G.-Z. Cao
Department of Materials Science & Engineering
University of Washington
Seattle, WA 98195, USA

DOI: 10.1002/admi.201600816

MoO_2, which is deemed to be a promising candidate for rechargeable LIBs, has been the subject of much research due to its high electrochemical activity toward Li^+.[14–16] Although bulk-sized MoO_2 usually has a low theoretical capacity (209 mA h g^{-1}), the lithiation of nanosized MoO_2 is a conversion-type reaction with a theoretical capacity 838 mA h g^{-1}.[17–19] As expected, all sorts of MoO_2 nanocomposites showed enhanced Li^+ storage performance.[18–20] But their disadvantages are blocking wider application, such as relatively low conductivity and huge volume change during lithiation/delithiation process. To overcome large volume change and slow kinetics during the lithiation/delithiation processes, one way was to synthesize nanosized MoO_2 to buffer the change of volume. Shi et al. have prepared ordered mesoporous MoO_2 which just displayed the capacity of 750 mA h g^{-1} at $C/20$ after 30 cycles.[17] Another more effective way was to prepare MoO_2 nanocomposites with different buffer phases of better cyclic stability, such as graphite and other carbon materials. A case in point is that Huang et al. have fabricated layer-by-layer assembled MoO_2–graphene thin film and achieved a specific capacity of 675.9 mA h g^{-1} after 100 cycles at 47.8 mA g^{-1}.[21] Yet the block of graphene sheets for ion diffusion cannot be completely overcome. Wei et al. synthesized MoO_2-ordered mesoporous carbon having a reversible capacity of 689 mA h g^{-1} in the 50th cycle at the current density of 50 mA g^{-1}.[15] However, the synthesis of ordered mesoporous carbon was not facile and its reversible capacity at 50 mA g^{-1} was not satisfactory.

According to the theoretical analysis,[22] the resistance polarization and concentration polarization are main reasons for the reversible capacity loss of electrode, especially the capacity loss at high current densities. Therefore, preparing MoO_2–carbon composites with fast electrons and ions transfer channels maybe result in the composites with excellent properties for Li^+ storage. Recently core shell nanostructures have been brought more and more attention in catalysis,[23] energy conversion and storage.[23,24] Core shell nanostructures can not only possess a short ions diffusion length, a high electrode/electrolyte interfacial area, and efficient electronic transport pathways, but also effectively

buffer the huge volume change of nanoparticles during the charge/discharge process. A number of different core shell nanostructures have been reported recently, including nanofibers,[25–29] nanospheres,[30–32] and nanorods.[33–35] According to our previous studies of carbon-fiber based composites[36–38] and some other researches,[39,40] nanofibers and their composites have better electron and Li^+ transport rates leading to a high contact area at the interface with the electrolyte and adapt to strain and volume varieties without any fracturing or fracking. Jang's group has developed core shell nanofibers using dual nozzle electrospinning with a gravimetric capacity retaining 721 mA h g^{-1} with a 5 min discharging rate capability after 300 cycles.[41] There are many similar core shell nanofibers obtained by coaxial electrospinning.[42,43] Although those methods lead to improved electrochemical properties, the multinozzle electrospinning needs complicated equipment and is hard to control the structure of the composites.

In this work, MoO_2@C core shell nanofibers have been prepared by a facile single nozzle electrospinning. The micromechanism of forming core shell nanofiber was studied by changing the annealing temperatures and the concentrations of the precursor. As a result, the MoO_2@C core shell nanofibers can deliver a high specific capacity of 665 mA h g^{-1} at 0.5 A g^{-1} after 600 cycles and coulombic efficiency has been maintained about 98%, even at 1 A g^{-1}, the capacity can possess 537 mA h g^{-1} after 600 cycles.

2. Results and Discussion

2.1. Formation of the MoO_2@C Core Shell Nanofibers

After annealing with a heating rate of 1 °C min^{-1} in flowing Ar, the morphology of the as-obtained product (MoO_2@C-10) at 650 °C can be clearly observed from the scanning electron microscopy (SEM) images in **Figure 1**a,b. And the more SEM images of MoO_2@C core shell nanofibers are showed in Figure S11 in the Supporting Information. It shows that the diameter of the nanofibers is about 500 nm and MoO_2 nanoparticles are coated by carbon layer to form MoO_2@C core shell nanofiber. X-ray diffraction (XRD) was used to examine MoO_2@C-10 in Figure 1c. Three characteristic peaks centered at 25.0°, 37.2°, and 53.6° are ascribed to the (011), (200), and (220) planes of MoO_2. The peak in 26° is displayed as graphite, which is gradually being the result of the graphitization and indicates that the electrode of MoO_2@C-10 is made to have a good conductivity. As shown in Figure 1d, Raman spectra of MoO_2@C-10, MoO_2@C-15 show two strong peaks at 1360 and 1600 cm^{-1}, representing the D-band (disordered carbon), the G-band (graphitic carbon), respectively. The intensity rate of the D-band and G-band (I_D/I_G) is regarded as a sign of crystallinity.[44] The numerical value of I_D/I_G is 0.93, 1.187 for the MoO_2@C-10, MoO_2@C-15 core shell nanofibers respectively, which indicates that the MoO_2@C-10 core shell nanofibers possess high degree of graphitization and better conductivity.[51]

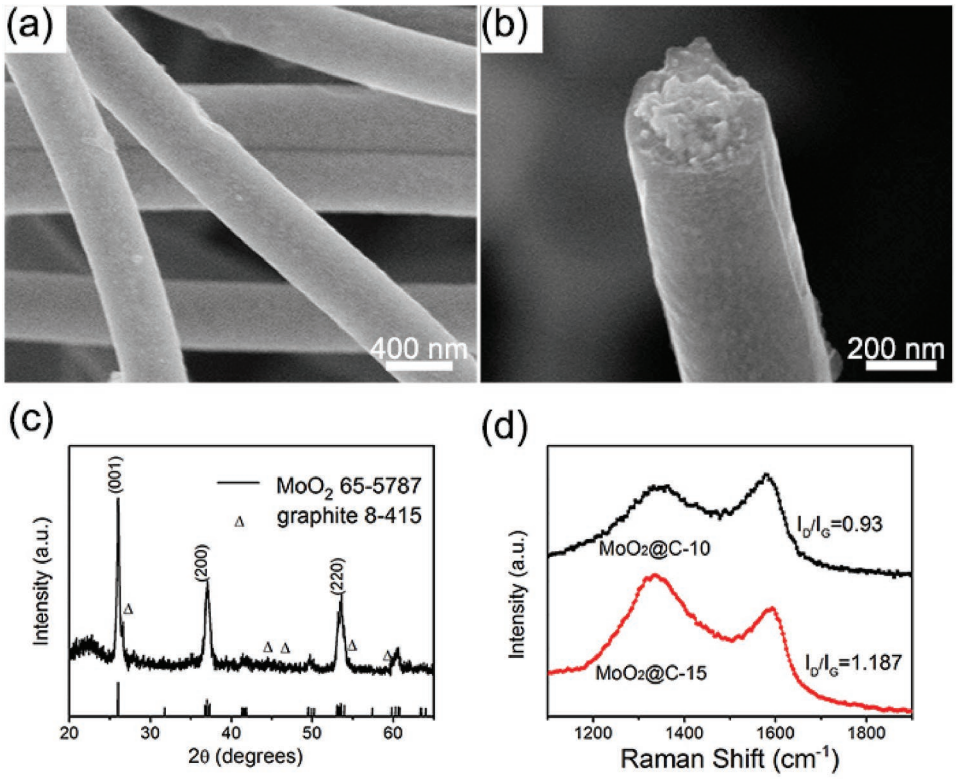

Figure 1. a,b) the SEM images of the MoO_2@C-10 core shell nanofibers at 650 °C with a heating rate of 1 °C min^{-1} in Ar. c) XRD patterns of the MoO_2@C-10 core shell nanofibers. d) Raman spectra of the MoO_2@C-10, MoO_2@C-15 core shell nanofibers, respectively.

The SEM and mappings of the as-electrospun nanofibers in Figure S1 (Supporting Information) indicate these elements(C, Mo, O) are uniformly dispersed in the nanofibers and draw a conclusion that the core shell nanofibers are formed during the annealing process.

2.2. Formation Mechanism of the MoO_2@C Core Shell Nanofibers

The precursor (a) (Figure S2, Supporting Information) was thermally analyzed by thermogravimetric analysis (TGA) with a heating rate of 5 °C min^{-1} in N_2. The weight losses (under 350 °C) were ascribed to the removal of adsorbed water, the polymer degradation,[45] and the conversion of ammonium molybdate (AMM) to MoO_3.[46] When increased to 450 °C, weight loss reached the maximum, which could mean that MoO_3 was gradually reduced to MoO_2.[15] After 450 °C, AMM was completely converted to MoO_2. The weight change (b) in Figure S2 in the Supporting Information with a heating rate of 5 °C min^{-1} in air was due to both the oxidation of MoO_2 and the decomposition of carbon layer. The theoretical value of the weight increases from MoO_2 to MoO_3 is 12.5 wt%. So the content of carbon in the MoO_2@C-10 core shell nanofibers was calculated to be about 37 wt%. The content of carbon in the MoO_2@C-15 core shell nanofibers was estimated to be about 23.89 wt%, as shown in Figure S2 in the Supporting Information.

In order to explain the mechanism of formating MoO_2@C core shell nanofibers, we characterize the distribution of MoO_2 nanoparticles at the cross section of the nanofibers obtained at different temperatures by SEM. The nanofibers were treated by ammonia to remove the MoO_2 nanoparticles and the resulted nanofibers were also observed. Figure S3a in the Supporting Information shows that the solid nanofibers are obtained under 300 °C and a hollow structure could be seen after ammonia water treatment, as shown in Figure S3b in the Supporting Information, which confirmed that MoO_2 nanoparticles was dispersed in the center of the nanofibers. When the heating temperature was increased to 400 °C, an obvious core shell nanofiber was formed in Figure S3c in the Supporting Information. Figure S3d in the Supporting Information showed that MoO_2 nanoparticles in the center were corroded, remaining a hollow carbon nanofiber. When increased to 500 °C, the diameter of MoO_2 nanoparticles enlarged and the carbon layer became relatively thinner in Figure S3e in the Supporting Information, which was likely that MoO_3 was further reduced to MoO_2. Hollow carbon nanotubes appeared after ammonia treatment in Figure S3f in the Supporting Information. From the above SEM images, it can be concluded that temperature is not the main factor to formate core shell nanofibers, but the high temperature is conducive to formate core shell nanofibers and can decrease the thickness of the carbon shell.

The effect of the concentrations of AMM on the structure of nanofibers was investigated in the formation mechanism of MoO_2@C core shell nanofibers, as shown in **Figure 2**. When the concentration of AMM was adjusted to 1%, solid nanofibers without nanoparticles were obtained. Although treated by ammonia water, there was no hollow structure in the nanofibers, indicating that MoO_2 nanoparticle was the homogenous distribution of the MoO_2 nanoparticles. When the concentration of AMM was increased to 5%, the center of the nanofibers showed some nanoparticles in. Then some small holes were in the nanofibers after the MoO_2 nanoparticles were dissolved in ammonia water. After the concentration of AMM was up to 10%, the core shell nanofiber was obvious and hollow carbon nanotube was achieved after removing the MoO_2 nanoparticles. When the concentration of AMM was increased to 15% further, the core shell nanostructure of MoO_2@C-15 nanofibers appeared more clearly in Figure S4 in the Supporting Information. As the concentrations increased, it could be concluded that MoO_2 nanoparticles formed priority in the center of the nanofibers and a relatively high concentration of AMM was the necessary condition to form the MoO_2@C core shell nanofibers using a single nozzle electrospinning.

To further explore the structure of the MoO_2@C core shell nanofibers, TEM was carried out. **Figure 3**a,b shows low magnification TEM images for the core shell nanofibers. It is clearly observed that MoO_2 nanoparticles are coated by carbon and relatively large nanoparticles are concentrated in the center

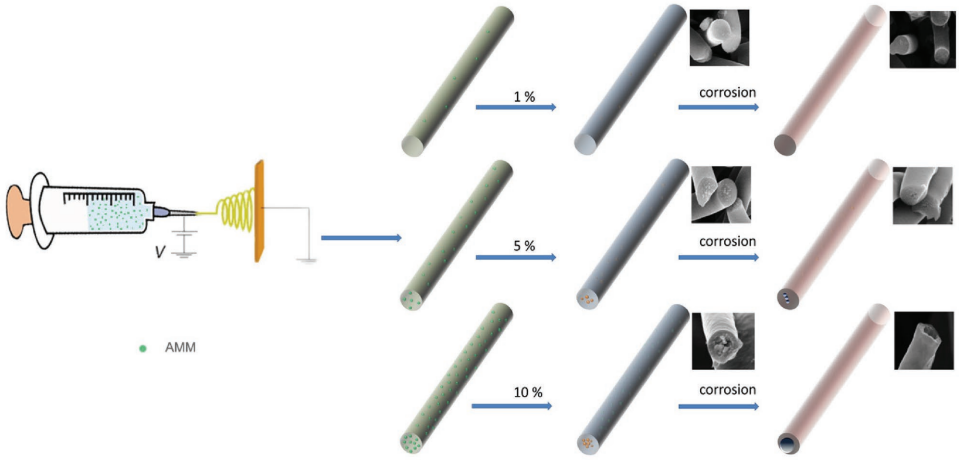

Figure 2. Schematic illustration of changes of MoO_2@C core shell nanofibers at different concentrations (1%, 5%, 10%), and after soaking in nitric acid, respectively.

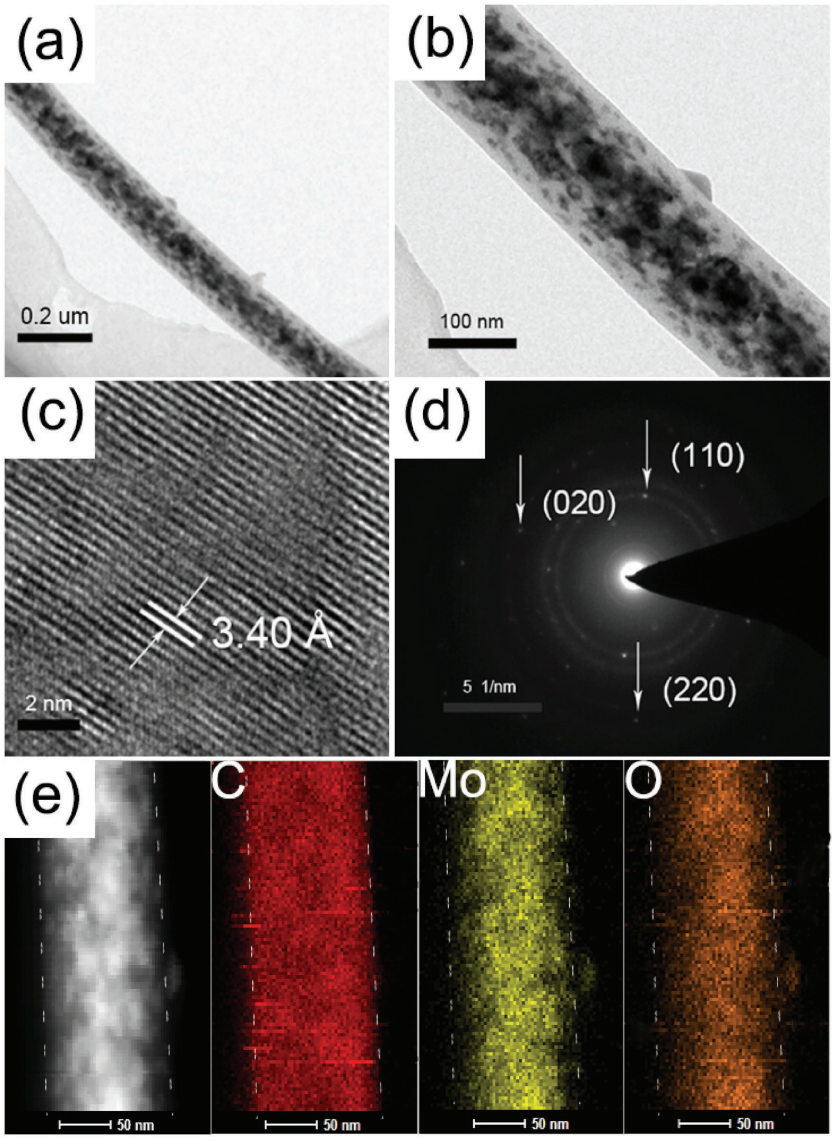

Figure 3. a,b) TEM image, c) HRTEM image, d) SAED pattern, e) dark field TEM, and corresponding element mappings for C, Mo, O of MoO_2@C core shell nanofibers.

of the nanofibers. And more TEM images of the MoO_2@C nanofibers are shown in Figure S12 in the Supporting Information. There may be the possibility of small particles combined into large particles during the annealing treatment. Besides, there is a tendency that nanoparticles aggregate into the core of the nanofibers. The lattice fringe (3.40 Å) is attributed to the (011) plane of MoO_2 (Figure 3c). The selected area electron diffraction (SAED) rings reveal the MoO_2 nanoparticles are polycrystalline (Figure 3d). The elemental mappings (Figure 3e) indicate that Mo and O are mainly distributed in the center of the nanofiber and most of C is at the edge of the nanofiber, confirming the core shell nanostructure of MoO_2@C composites from another angle.

A series of optical tests were reformed to explore the formation mechanism of MoO_2@C core shell nanofibers. First, polyvinyl alcohol (PVA) and AMM were mixed to get a uniform and transparent solution in Figure S5a in the Supporting Information, showing the macroscopic homogeneity. Figure S5b in the Supporting Information is optical image of pure PVA solution (after drying) by optical microscope indicating the uniformity of PVA. When the concentration of AMM is 1%, the optical image in Figure S5c in the Supporting Information suggests that AMM is uniformly dispersed in PVA solution. When the concentration of AMM is added to 10% (dry at 60 °C), clear spots appear in Figure S5d in the Supporting Information, showing that AMM with a concentration of 10 wt% cannot be dissolved completely in PVA. Compared to the optical images of AMM/PVA with different ratios, it can be found that there is the phase segregation phenomenon when the weight ratio of AMM was 10%. When the precursor solution (AMM in 10%) is respectively annealed at 120 and 240 °C, the optical images indicate that the particles aggregate and become larger in Figure S6 in the Supporting Information. It is the aggregation of particles that are affected by thermodynamics.

Therefore the formation of MoO_2@C core shell nanofibers can be ascribed to the phase-segregation in the PVA/AMM mixture with the increase ratio of AMM. The mappings of the as-electrospun nanofibers in Figure S1 in the Supporting Information show that C, Mo, O are uniformly dispersed in the nanofibers and the core shell nanofibers are formed during the annealing process. A small amount of AMM (1 wt%) can be dissolved absolutely in PVA to form a homogenous solution and cannot result in core shell nanostructure in MoO_2@carbon composites. As the increase of the AMM ratio in the mixture, only a part of AMM can be dissolved and other AMM form nanoparticles in the PVA matrix. Because the PVA was the primary component, AMM nanoparticles were embedded in the center of PVA nanofibers. During the annealing treatment, MoO_3 from AMM were reduced by surrounding PVA and corresponding carbon, resulting in the removal of carbon layers among MoO_2 nanoparticles in the center and the aggregation of MoO_2 nanoparticles in the center of nanofibers.

2.3. Electrochemical Performances of the MoO_2@C Core Shell Nanofibers

The electrochemical properties of the MoO_2@C core shell nanofibers were investigated. The cyclic voltammetry (CV) curves of MoO_2@C at a sweep rate of 0.5 mV s^{-1} between 0 and 3.0 V are shown in **Figure 4**a. During the first cycle, there was no obvious reduction peak, which is insertion-type reaction,[21] irreversible reduction of the electrolyte, and the formation

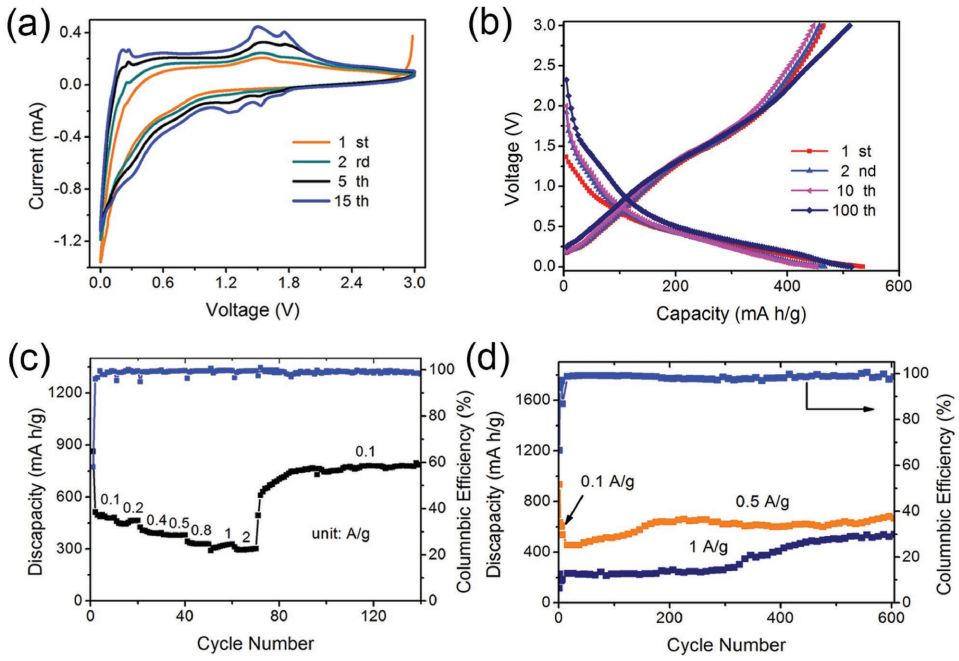

Figure 4. a) CV curves of MoO_2@C-10 core shell nanofibers between 0 and 3.0 V at the sweep speed of 0.5 mV s^{-1}. b) Charge–discharge curves of MoO_2@C-10 core shell nanofibers at a current density of 500 mAg $^{-1}$. c) Rate performance of MoO_2@C-10 core shell nanofibers at a current density of 0.1, 0.2, 0.4, 0.5, 0.8, 1, and 2 A g^{-1}, respectively. d) Cycling performances of MoO_2@C-10 core shell nanofibers at a current density of 0.5 and 1 A g^{-1}, respectively.

of the passivating surface film.[47,48] From the second cycle onward, the area of the CV profiles is increasing, which indicates the high reversibility during Li^+ insertion/extraction. Two pronounced redox peaks (1.52/1.75 V and 1.23/1.50 V) are associated with the reversible phase transitions of Li_xMoO_2.[49,50] Over 1.0 V, Li^+ is inserted into the lattice of MoO_2, which formates Li_xMoO_2. When the potential is discharged below 1.0 V, Li_xMoO_2 would slowly convert to Mo and Li_2O. With the charge discharge, the oxidation peaks form graphite of less than 0.3 V, which is more obvious and shows that MoO_2@C-10 possesses good electrochemical performance in the process of charge discharge.[51]

Figure 4b shows the galvanostatic charge discharge curves for MoO_2@C-10 electrode at 0.5 A g^{-1} between 0 and 3.0 V. It can be drawn that the coulombic efficiency of the first cycle is 86.78%. The capacity loss (13.22%) of the first cycle is ascribed to the irreversible reasons, including the decomposition of the electrolyte, the formation of solid electrolyte interface (SEI), and the trapping of Li into the lattice of MoO_2.[[18] From the 10th cycle, the capacity of the electrode increases gradually.

The rate capacity of MoO_2@C core shell nanofiber electrode is used to investigate the rate capacity. Figure 4c shows the rate capacity of MoO_2@C core shell nanofiber electrode tested at 0.1, 0.2, 0.4, 0.5, 0.8, 1, 2 A g^{-1}. The initial capacity of 0.1 A g^{-1} possesses 863 mA h g^{-1}, even at the current density of 2 A g^{-1}, the electrode still remains 312 mA h g^{-1}. When the current density is back to 0.1 A g^{-1}, the capacity gradually increased to 753 mA h g^{-1}, due to infiltration of electrolyte and activation of materials,[16,17] which is the maximum capacity.

The cycling performances of the MoO_2@C core shell nanofibers at a current density of 0.5, 1 A g^{-1} are shown in Figure 4d. Within the subsequent cycles, the discharge capacity of the core shell nanofibers gradually increases, respectively. This result is ascribed to the activation of the electrodes, which is consistent with the CV measurement.[15] In the 600th cycle, the discharge capacity still maintained 665 mA h g^{-1}. The core shell nanofibers also show a good coulombic efficiency, which is close to 100% in the cycles shown in Figure 4c,d. Even after 600 cycles at 1 A g^{-1}, it still has a capacity of 537 mA h g^{-1}. Compared with other MoO_2 based materials (Table S1, Supporting Information), the MoO_2@C core shell nanofibers by single nozzle electrospinning also show excellent cycling performance and high capacity in the process of the charge discharge. As a comparison, hollow carbon electrode displays a good stability cycle in Figure S7 in the Supporting Information. Although the capacity discharge of MoO_2@C-15 can be reached to 500 mA h g^{-1}, which may be due to permeation of electrolyte and activation of materials,[15] decay rate is too bad. From Figure S2 in the Supporting Information, the content of MoO_2 in MoO_2@C-15 is higher than that in MoO_2@C-10. It could be a very important factor causing the rupture of the MoO_2@C-15 core shell nanofibers, as shown in Figure S9b in the Supporting Information. In Figure S9a in the Supporting Information, the complete nanowires still existed in MoO_2@C-10 electrodes. It is also shown that the MoO_2@C-10 core shell nanofibers have a good stability. The excellent cycling properties of MoO_2@C nanofibers were closely related to such reasons. First, the unique core shell nanofibers effectively not only maintain the integrity of the structure but also suppress the volume expansion of MoO_2. Second, the graphitized carbon in the nanofibers can improve the conductivity of the electrode. Third, diffusion time of the Li^+ diffusion in electrode materials

can be effectively shortened by nanosize MoO_2@C.[52] Fourth, the core shell nanofibers may significantly minimize ohmic and concentration/activation polarization to improve electronic and ionic transport rates.[51] MoO_2@C-10 core shell nanofibers are tried to use as sodium negative electrode and investigated the discharge capacity (Figure S10, Supporting Information). However, the performance is poor, the possible reason is that sodium ion radius is greater than Li^+ and the intercalation/deintercalation is difficult.

3. Conclusion

MoO_2@C core shell nanofibers were obtained by electrospinning with a single nozzle. Through a series of electron microscopic images, the formation principle of the core shell structure is well explained. The MoO_2@C core shell nanofibers can accommodate the huge volume variation of nanoparticles and possess a short ion solid diffusion length, a high electrode/electrolyte interfacial area, which demonstrated excellent electrochemical properties. For example, the product exhibited high specific capacity of 655 mA h g^{-1} for 600 cycles at a current density of 0.5 A g^{-1} and good rate capability and reversibility. Even when the current density was up to 1 A g^{-1}, the capacity still has 537 mA h g^{-1} after 600 cycles. In this paper, a more simple method for the synthesis of core shell nanostructure is introduced to research other metal oxide/carbon core shell nanostructures.

4. Experimental Section

Preparation of Materials: All chemicals were of analytical grade and used without further purification. MoO_2@C core shell nanofibers were obtained by a facile single nozzle electrospinning with a subsequent annealing. A typical process is as follows: AMM tetrahydrate ($(NH_4)_6Mo_7O_{24}{\cdot}4H_2O$, 99%) was dissolved in deionized water (10 g), then PVA (M_w = 80 000, 1 g) was mixed in water at 60 °C for 8 h, lastly a transparent solution of PVA/AMM was acquired. The above precursor solution was put into a syringe. At the constant speed of 0.4 mL h^{-1}, the voltage of 17 kV was applied between the electrospinning jet and the collector (16 cm), then the precursor solution was electrospun into nanofibers. The as-electrospun nanofibers were dried at 60 °C for overnight in vacuum drying box, then annealed at 650 °C for 4 h with a heating rate of 1 °C min^{-1} in Ar. The products of AMM in 10%, 15% were named MoO_2@C-10, MoO_2@C-15, respectively. Another contrast, hollow carbon was obtained by MoO_2@C-10 soaked in ammonia water (25%) for 12 h after drying.

Characterization: The sample was characterized using XRD, a SEM (Hitachi S4-800), a transmission electron microscope (TEM, JEOL-2010), TGA, and Raman spectroscopy (laser wavelength of 512 nm).

Electrochemical Measurements: The electrochemical measurements were done using CR2025-type coin cells. In order to obtain a homogeneous mucus, active materials (MoO_2@C-10, 80 wt%), conductivity agent carbon black (10 wt%), binder carbonxymethyl cellulose (CMC) (10 wt%) were mixed in distilled water, then stirred for 8 h. Then the mixed gel was applied onto a copper foil and dried at 60 °C in a vacuum oven overnight. The electrolyte contained a solution of 1 M $LiPF_6$ in ethylene carbonate, diethyl carbonate, and dimethyl carbonate (1:1:1, w/w). These cells were assembled in the glovebox filled with highly pure argon gas (O_2 and H_2O levels less than 0.05 ppm). CV was obtained on a Chen Hua CHI 660E electrochemical workstation. The charge/discharge measurements were carried out on an Arbin BT2000 system with the potential window of 0–3 V. As a contrast, the cycling performances of MoO_2@C-15 and CTBs electrodes were tested under the same environment.

Supporting Information

Supporting Information is available from the Wiley Online Library or from the author.

Acknowledgements

The present work was supported by the National Natural Science Foundation of China (Grants 51404103, 51574117, and 61376073), Hunan University Fund for Multidisciplinary Developing (2015JCA04), and Fundamental Research Funds for the Central Universities. This work was also in part financially supported by the National Science Foundation (NSF, DMR 1505902).

Received: August 22, 2016
Revised: September 26, 2016
Published online: December 1, 2016

[1] W. Zhou, C. Cheng, J. Liu, Y. Y. Tay, J. Jiang, X. Jia, J. Zhang, H. Gong, H. H. Hng, T. Yu, *Adv. Funct. Mater.* **2011**, *21*, 2439.
[2] M. S. Whittingham, *Chem. Rev.* **2004**, *104*, 4271.
[3] L. Huang, D. Chen, Y. Ding, Z. L. Wang, Z. Zeng, M. Liu, *ACS Appl. Mater. Interfaces* **2013**, *5*, 11159.
[4] J. Liu, Y. Wen, Y. Wang, P. A. van Aken, J. Maier, Y. Yu, *Adv. Mater.* **2014**, *26*, 6025.
[5] X. Wang, B. Liu, X. Hou, Q. Wang, W. Li, D. Chen, G. Shen, *Nano Res.* **2014**, *7*, 1073.
[6] L. Li, B. Peng, Z. Tao, F. Cheng, J. Chen, *Adv. Funct. Mater.* **2010**, *20*, 1894.
[7] K. T. Nam, D.-W. Kim, P. J. Yoo, C.-Y. Chiang, N. Meethong, P. T. Hammond, Y.-M. Chiang, A. M. Belcher, *Science* **2006**, *312*, 885.
[8] Z. Hong, M. Wei, T. Lan, L. Jiang, G. Cao, *Energy Environ. Sci.* **2012**, *5*, 5408.
[9] Y. Zhong, X. Wang, K. Jiang, J. Y. Zheng, Y. Guo, Y. Ma, J. Yao, *J. Mater. Chem.* **2011**, *21*, 17998.
[10] T. Yang, Y. Chen, B. Qu, L. Mei, D. Lei, H. Zhang, Q. Li, T. Wang, *Electrochim. Acta* **2014**, *115*, 165.
[11] F.-F. Cao, Y.-G. Guo, L.-J. Wan, *Energy Environ. Sci.* **2011**, *4*, 1634.
[12] G. Zhang, H. B. Wu, H. E. Hoster, X. W. Lou, *Energy Environ. Sci.* **2014**, *7*, 302.
[13] C. Guan, D. Chao, Y. Wang, J. Wang, J. Liu, *Part. Part. Syst. Charact.* **2016**, *33*,1521.
[14] Y. Sun, X. Hu, C. Y. Jimmy, Q. Li, W. Luo, L. Yuan, W. Zhang, Y. Huang, *Energy Environ. Sci.* **2011**, *4*, 2870.
[15] H. J. Zhang, K. X. Wang, X. Y. Wu, Y. M. Jiang, Y. B. Zhai, C. Wang, X. Wei, J. S. Chen, *Adv. Funct. Mater.* **2014**, *24*, 3399.
[16] Y. Wang, Z. Huang, Y. Wang, *J. Mater. Chem. A* **2015**, *3*, 21314.
[17] J. Ni, Y. Zhao, L. Li, L. Mai, *Nano Energy* **2015**, *11*, 129.
[18] Q. Tang, Z. Shan, L. Wang, X. Qin, *Electrochim. Acta* **2012**, *79*, 148.
[19] Y. Liu, H. Zhang, P. Ouyang, Z. Li, *Electrochim. Acta* **2013**, *102*, 429.
[20] X. Zhao, M. Cao, B. Liu, Y. Tian, C. Hu, *J. Mater. Chem.* **2012**, *22*, 13334.
[21] F. Xia, X. Hu, Y. Sun, W. Luo, Y. Huang, *Nanoscale* **2012**, *4*, 4707.
[22] M. Winter, R. J. Brodd, *Chem. Rev.* **2004**, *104*, 4245.
[23] Y. Z. Chen, Q. Xu, S. H. Yu, H. L. Jiang, *Small* **2015**, *11*, 71.

[24] F. Wang, R. Deng, J. Wang, Q. Wang, Y. Han, H. Zhu, X. Chen, X. Liu, *Nat. Mater.* **2011**, *10*, 968.
[25] F. Yan, X. Tang, Y. Wei, L. Chen, G. Cao, M. Zhang, T. Wang, *J. Mater. Chem. A.* **2015**, *3*, 12672.
[26] X. Lu, M. Yu, G. Wang, T. Zhai, S. Xie, Y. Ling, Y. Tong, Y. Li, *Adv. Mater.* **2013**, *25*,267.
[27] H. Kim, J. Cho, *Nano Lett.* **2008**, *8*, 3688.
[28] R. Li, Z. Lin, X. Ba, Y. Li, R. Ding, J. Liu, *Nanoscale Horizons* **2016**, *1*, 150.
[29] C. Wang, L. Wu, H. Wang, W. Zuo, Y. Li, J. Liu, *Adv. Funct. Mater.* **2015**, *25*, 3524.
[30] R. Li, Y. Wang, C. Zhou, C. Wang, X. Ba, Y. Li, X. Huang, J. Liu, *Adv. Funct. Mater.* **2015**, *25*, 5384.
[31] H. Sun, X. Sun, M. Yu, A. K. Mishra, L. Huang, J. Lian, *Adv. Funct. Mater.* **2014**, *24*, 2389.
[32] D. Yu, C. Chen, S. Xie, Y. Liu, K. Park, X. Zhou, Q. Zhang, J. Li, G. Cao, *Energy Environ. Sci.* **2011**, *4*, 858.
[33] G. Zhang, S. Hou, H. Zhang, W. Zeng, F. Yan, C. C. Li, H. Duan, *Adv. Mater.* **2015**, *27*, 2400.
[34] R. Li, X. Ren, F. Zhang, C. Du, J. Liu, *Chem. Commun.* **2012**, *48*, 5010.
[35] Y. Yao, M. T. McDowell, I. Ryu, H. Wu, N. Liu, L. Hu, W. D. Nix, Y. Cui, *Nano Lett.* **2011**, *11*, 2949.
[36] X. Tang, F. Yan, Y. Wei, M. Zhang, T. Wang, T. Zhang, *ACS Appl. Mater. Interfaces* **2015**, *7*, 21890.
[37] Y. Wei, F. Yan, X. Tang, Y. Luo, M. Zhang, W. Wei, L. Chen, *ACS Appl. Mater. Interfaces* **2015**, *7*, 21703.
[38] X. Zhang, Z.-A. Qiao, Z. Zhang, S. Wana, S. Dai, *J. Mater. Chem. A* **2014**, *120*, 110.
[39] X. Jia, Z. Chen, A. Suwarnasarn, L. Rice, X. Wang, H. Sohn, Q. Zhang, B. M. Wu, F. Wei, Y. Lu, *Energy Environ. Sci.* **2012**, *5*, 6845.
[40] Y. Gong, M. Zhang, G. Cao, *RSC Adv.* **2015**, *5*, 26521.
[41] T. H. Hwang, Y. M. Lee, B.-S. Kong, J.-S. Seo, J. W. Choi, *Nano Lett.* **2012**, *12*, 802.
[42] X. Xia, X. Wang, H. Zhou, X. Niu, L. Xue, X. Zhang, Q. Wei, *Electrochim. Acta.* **2014**, *121*, 345.
[43] J. Kong, W. A. Yee, Y. Wei, L. Yang, J. M. Ang, S. L. Phua, S. Y. Wong, R. Zhou, Y. Dong, X. Li, *Nanoscale* **2013**, *5*, 2967.
[44] K.-J. Kim, T.-S. Lee, H.-G. Kim, S.-H. Lim, S.-M. Lee, *Electrochim. Acta* **2014**, *135*, 27.
[45] X. Yang, C. Shao, H. Guan, X. Li, J. Gong, *Inorg. Chem. Commun.* **2004**, *7*, 176.
[46] W. Shaheen, M. Selim, *J. Therm. Anal. Calorim.* **2000**, *59*, 961.
[47] Z. Xu, H. Wang, Z. Li, A. Kohandehghan, J. Ding, J. Chen, K. Cui, D. Mitlin, *J. Phys. Chem. C* **2014**, *118*, 18387.
[48] D. Koziej, M. D. Rossell, B. Ludi, A. Hintennach, P. Novák, J. D. Grunwaldt, M. Niederberger, *Small* **2011**, *7*, 377.
[49] B. Guo, X. Fang, B. Li, Y. Shi, C. Ouyang, Y.-S. Hu, Z. Wang, G. D. Stucky, L. Chen, *Chem. Mater.* **2012**, *24*, 457.
[50] X. Liu, W. Ji, J. Liang, L. Peng, W. Hou, *Phys. Chem. Chem. Phys.* **2014**, *16*, 20570.
[51] Y. Tang, Y. Zhang, W. Li, B. Ma, X. Chen, *Chem. Soc. Rev.* **2015**, *44*, 5926.
[52] J. Zhang, Z. Xie, W. Li, S. Dong, M. Qu, *Carbon* **2014**, *74*, 153.

